Modelling oil droplet/film interaction in an aero-engine bearing chamber

M Farrall, S Hibberd, K Simmons

The University of Nottingham Technology Centre in Gas Turbine Transmission Systems, University Park, Nottingham, NG7 2RD, UK.

A composite numerical model, based on a commercial CFD package, is presented for use in predicting the complex two-phase air/oil flow in aero-engine bearing chambers. The code CFX-4.3 is used to calculate the airflow and oil droplet trajectories in a typical aero-engine bearing chamber with sub-models incorporated to describe the oil film motion and interaction of the oil droplets with this film. The numerical results show that droplets shed from the bearing cage will have sufficient energy on impact with the wall film to promote splashing. Moreover, preliminary results show good qualitative agreement with existing experimental data in the literature. The study identifies that the inclusion of droplet/film interactions is necessary to obtain accurate results when simulating two-phase flows in bearing chambers.

1. Introduction

The oil lubrication system forms an integral part of the modern aero-engine, and with future designs seeking increases in shaft speeds and sealing air temperatures the need to optimise this system becomes ever more important. Bearing chambers are components within this system that provide a modelling challenge as they contain a complex two-phase air and oil flow. The bearing chamber used to develop the modelling methodology in this work is that currently being studied experimentally at the Institut für Thermische Strömungsmachinen (ITS), University of Karlsruhe, as part of the European funded project ATOS[1]. The chamber is formed by a combination of high speed rotating, typical speeds being 10000 rpm, and stationary walls inducing a strong azimuthal component of flow. This flow is modified by the presence of flow inlets, through an axisymmetric bearing and seal, and flow outlets, through vent and scavenge pipes. Cross sections through the chamber studied, taken at an axial position corresponding to the middle of the chamber and at an angular location corresponding to the position of the vent pipe, are shown schematically in Fig. 1. Oil is supplied to the roller bearing for lubrication and as a result discrete oil droplets are ejected into the rotating airflow. Due to the angular momentum transferred to the droplets from the bearing and associated bearing cage the droplets ultimately impinge on the outer chamber housing. The outcome of the impingement may result in immediate deposition, in which case a wall film is usually formed that migrates round the chamber.

[1] ATOS – Advanced Transmission and Oil System concepts

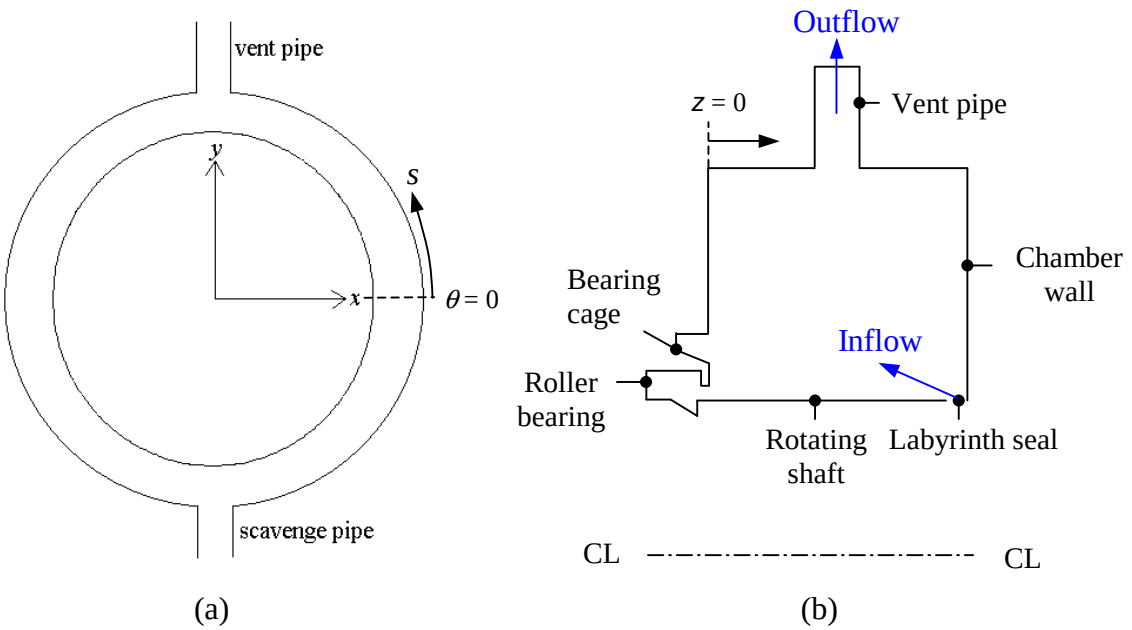

Figure 1. Schematic showing chamber cross section through (a) $z = 0.022$, (b) $x = 0$.

Alternatively, droplets may break-up on impact with smaller droplets being ejected back into the airflow and further impingement may occur.

The two-phase flow in a similar geometry has been studied extensively in the past, with work focused on the oil film motion [1,2,3,4,5] and heat transfer [1,2,6,7]. The variation in the oil film thickness with angular location and the velocity profile in the film have been measured experimentally by Wittig et al. [1] and Glahn and Wittig [2] respectively. A two-dimensional analytic model was developed for the film flow by balancing the forces on the fluid and assuming a form for the shear stress within the film [2]. Good agreement was obtained when compared to the experimental data for the velocity profile. The force balance approach was also adopted by Chew [4] to study the effect of mass and momentum transfer to the oil film from impinging droplets. The analysis used simple axisymmetric source terms for the contributions of mass and momentum. Whilst yielding information about the dynamics of the oil film these models are limited for most engineering applications as knowledge of the flow is assumed in the calculations. Farrall et al [5,8] developed a global modelling methodology using a CFD calculation to provide information regarding the distribution of the interfacial shear, mass and momentum to the film.

The interaction of oil droplets with any film present on the chamber housing is also an important aspect when modelling the two-phase flow in bearing chambers. Little direct experimental data exist for bearing chambers at present, but analogous cases are the characterisation of secondary droplets in DI diesel engines [9,10,11,12,13] and in pre-film atomisers [14,15,16]. Information from these studies was used by Farrall [8] to develop a two-dimensional model for the interaction of oil droplets with an oil film for a simplified bearing chamber. The model was incorporated into CFX-4.3 and shown to be capable of predicting valuable information on the change in droplet diameters within the rotating core airflow as a result of break-up. This paper develops an extended three-dimensional model for film flow to enable simulation of droplet/film interaction in actual bearing chamber geometries and operating conditions.

2. Nomenclature

d	[m]	droplet diameter
f	[-]	friction factor
g	[ms^{-2}]	gravity
h	[m]	film thickness
k	[m^2s^{-2}]	turbulent kinetic energy
K	[-]	impact parameter
$\dot{M}$	[ms^{-1}]	Volume flow rate per unit area
$\dot{G}$	[m^2s^{-2}]	Circumferential momentum flow rate per unit area
$\dot{H}$	[m^2s^{-2}]	Axial momentum flow rate per unit area
q	[m^2s^{-1}]	circumferential volume flow rate per unit length
Q	[m^2s^{-1}]	axial volume flow rate per unit length
Re_f	[-]	Reynolds number
Re_d	[-]	Reynolds number, $\frac{\rho d u_n}{\mu}$
s	[m]	circumferential coordinate
t	[s]	time
u	[ms^{-1}]	velocity
We_d	[-]	Weber number, $\frac{\rho d u_n^2}{\sigma}$
z	[m]	axial coordinate

Greek symbols

λ	[-]	exit flow parameter
μ	[$kgm^{-2}s$]	dynamic viscosity
θ	[rad]	angle
ρ	[kgm^{-3}]	density
σ	[Nm^{-1}]	surface tension
τ	[kgm^{-2}]	shear stress
ψ	[rad]	in-plane turning angle

Subscripts

n	normal component
s	local tangent component
w	wall
z	axial component

3. The computational model

The model employs the commercial CFD package CFX-4.3 to calculate the core airflow and the trajectories of the oil droplets in the chamber. It is assumed that no air exits through the scavenge pipe and thus modelling of this geometric feature is omitted in the CFD calculation of the airflow. The oil is assumed to be released from the bearing cage as droplets and their motion solved numerically using a Lagrangian particle tracking method. At this stage in the study the droplets are modelled as rigid spheres with collisions between droplets, and turbulent dispersion neglected. Moreover, it is expected that the modification of the airflow by the oil droplets momentum will only affect the motion of very small droplets that will exit the chamber through the vent pipe and thus has been omitted in this study. Sub-models to describe the motion of the oil film present on the outer wall of the chamber and the interaction of the oil droplets with the oil film have been developed and incorporated into the model.

The simulation for the two-phase flow is implemented in successive stages. Firstly, the airflow in the chamber is calculated using CFX-4.3. Oil droplets are then tracked through the chamber, employing the droplet/film interaction model where necessary. Finally, droplet data are gathered for the input of mass and momentum to the oil film. These data are used together with a computed distribution of surface shear to provide required boundary information to the oil film model.

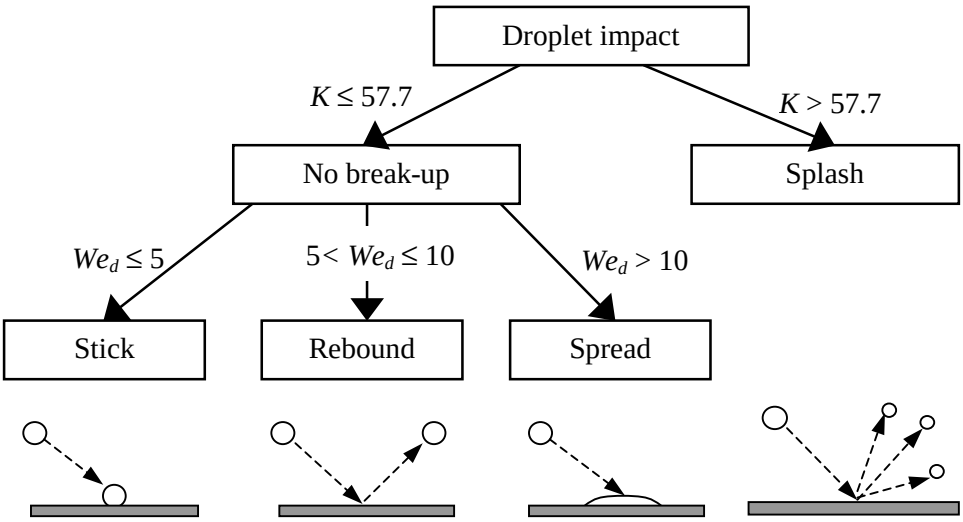

Figure 2. Schematic showing the structure of droplet/film interaction model and the transition criteria for the various outcomes.

3.1 Droplet/film interactions

The confined nature of aero-engine bearing chambers and high speed core airflow mean that oil droplet/film interactions are an important phenomenon and affect the size distribution of the droplets within the airflow as well as the heat transfer within the chamber. The model developed by Farrall [8], for flow in a simplified bearing chamber, is used to account for the effects of droplet impacts with the oil film. Classification is divided primarily on whether the droplet breaks up on impact with the oil film, and is evaluated according to a correlation based on the splashing parameter $K\left(= We_d^{0.5}\,\mathrm{Re}_d^{0.25}\right)$. If the droplet does not **splash** the impact is further classified into the regimes of **stick**, **rebound** and **spread**, shown schematically in Fig. 2 together with the associated parameter values. For specific details on the calculation of the post-impingement characteristics the reader is referred to Farrall [8].

To enable three-dimensional droplet impacts to be simulated, the in-plane turning angle, ψ, for droplets that are ejected back into the core flow needs to be calculated. The angle ψ is defined as the angle through which a droplet may turn on the film surface with respect to the tangential velocity vector of the impinging droplet. In the present work this angle is determined using the model suggested by Naber and Reitz [9].

3.2 Oil film motion

Oil is deposited on the stationary chamber housing as a result of oil droplet impacts, and forms a wall film that migrates around the chamber. To include the dynamics of this wall film, the model developed Farrall et al. [5] has been extended from a circumferential model to include variations in the axial direction. The model accounts for the effects of gravity, shear forces on both the wall and the films surface, and the addition of mass and momentum to the film from impinging oil droplets. Model equations have been derived for an incompressible, isothermal flow using a lubrication approximation for the film thickness, h, azimuthal volume flux, q, and axial volume flux, Q, and are given by

$$\frac{dh}{dt} + \frac{\partial q}{\partial s} + \frac{\partial Q}{\partial s} = \dot{M}\,, \tag{3}$$

$$\frac{dq}{dt}+\frac{\partial}{\partial s}\left[\frac{q^2}{h}-\frac{1}{2}gh^2\sin\theta\right]+\frac{\partial}{\partial z}\left[\frac{qQ}{h}\right]=\frac{1}{\rho}\left[\tau_s-\tau_{w,s}\right]-g\cos\theta+\dot{G}\,, \tag{4}$$

$$\frac{dQ}{dt}+\frac{\partial}{\partial s}\left[\frac{qQ}{h}\right]+\frac{\partial}{\partial z}\left[\frac{Q^2}{h}-\frac{1}{2}gh^2\sin\theta\right]=\frac{1}{\rho}\left[\tau_z-\tau_{w,z}\right]+\dot{H}\,. \tag{5}$$

The model is based on a local coordinate system that is normal and tangential to the wall. The axial coordinate, *z*, is taken to be zero at the wall nearest the bearing and increases in the direction of the seal. The circumferential coordinate, *s*, is taken to be 0 on the positive *x* axis (see Fig. 1(a)) and increases in an anticlockwise direction. The wall shear, τ_w, in equations (4) and (5) is modelled assuming that the shear is directly proportional to the square of the mean film velocity and is given by

$$\tau_{w,s}=\frac{1}{2}f_s\left(\frac{q}{h}\right)^2,\ f_s=\frac{4}{\mathrm{Re}_f},\mathrm{Re}_f=\frac{\rho hq}{\mu}, \tag{6}$$

$$\tau_{w,z}=\frac{1}{2}f_z\left(\frac{Q}{h}\right)^2,\ f_z=\frac{4}{\mathrm{Re}_f},\mathrm{Re}_f=\frac{\rho hQ}{\mu}. \tag{7}$$

The distribution of the mass/momentum added to the film as a result of droplet impingement is calculated using data regarding the loss of mass/momentum during the impact, obtained from the droplet/film interaction model.

For numerical calculations, equations (3) to (5) are discreitsed on a trapezoidal computational domain according to the scheme of Liska and Wendroff [17], allowing for accurate representation of the circular vent pipe boundary. Conditions applied on the side and end walls of the chamber are given by

$$\frac{\partial^2 h}{\partial n^2}=\frac{\partial q}{\partial n}=\frac{\partial Q}{\partial n}=0. \tag{8}$$

Oil exiting the chamber is given by a local analysis where the volume flux at the vent pipe boundary is proportional to the local gradient in the volume flux, i.e.

$$\frac{\partial h}{\partial n}=0,\frac{\partial \mathbf{F}}{\partial n}=-\lambda\mathbf{F},\mathbf{F}=[q,Q]. \tag{9}$$

The parameter λ is taken to represent the local geometrical flow conditions prevailing to the vent pipe. The numerical solution is based on a FORTRAN code for the film flow and has been incorporated into the CFD model of the bearing chamber.

4. Results and discussion

The composite numerical model, combining the CFD model, the droplet/film interaction model and the wall film model, has been used to simulate the steady state, two-phase air/oil flow in the bearing chamber under engine operating conditions. The chamber geometry is discretised using a body-fitted, structured computational domain and the airflow calculated using the *k-ε* turbulence model. Air, having a density of 2.923 $\mathrm{kgm^{-3}}$ and a dynamic viscosity of 1.837×10^{-5} $\mathrm{kgm^{-1}s^{-1}}$, enters the chamber through the seal; the air taken to enter the chamber at an angle of 75^{o} (measured from the normal to the rotating shaft) with a tangential component of velocity equal to 25% that of the rotating shaft speed. The roller bearing and

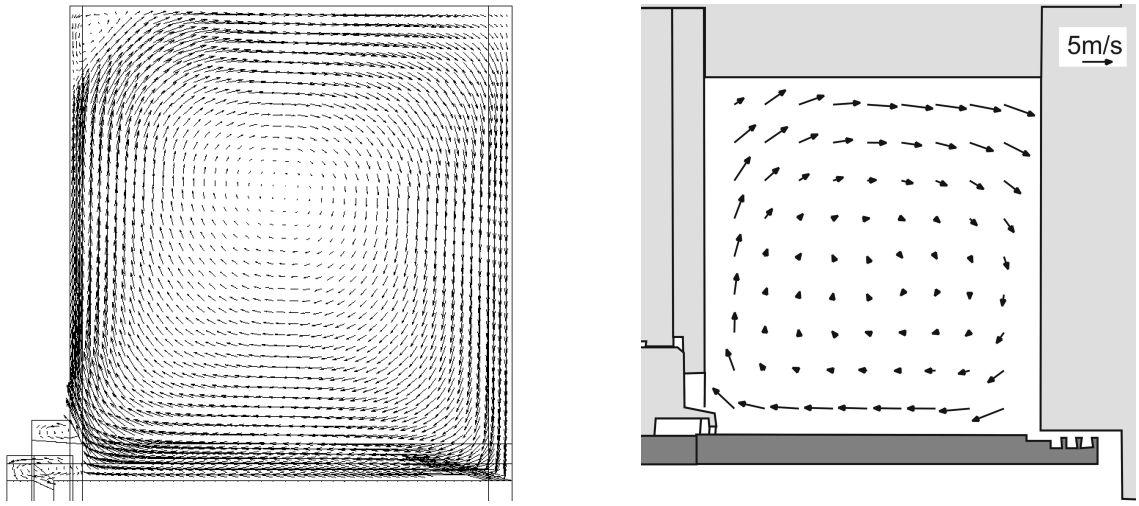

(a) (b)

Figure 3. Vector plots of the secondary airflow at an angular location corresponding to 90^o downstream of the vent pipe; (a) Numerical prediction, (b) Experimental data.

associated cage are taken to rotate at half the angular speed of the shaft with leakage of air through the bearing being neglected at this stage. Preliminary results have been obtained for a shaft speed of 9726 rpm and a sealing flow rate of 1.69×10^{-2} kgs^{-1}. Oil, having a density of 954 kgm^{-3} and a dynamic viscosity of 9.5×10^{-3} kgm^{-1}s^{-1}, is released in the form of droplets from 10 locations, equally spaced around the bearing cage, with a total mass flow rate of oil of 1.0×10^{-3} kgs^{-1} being ejected into the chamber. Using previous experimental results [18] the diameters are taken to satisfy a Rossin-Rammler distribution with a mean diameter of 100μm and spread parameter of 2. The droplets are ejected with an initial azimuthal component of velocity equal to that of the bearing cage, and an axial component of velocity equal to 5 ms^{-1}. For the purpose of the this simulation the oil film on the chamber housing is assumed to have a volume flow rate of 1.0×10^{-4} m^{3}s^{-1} in the azimuthal direction prior to any droplet impact and the exit parameter λ is given a value of 0, corresponding physically to an unrestricted exit flow.

The airflow in the chamber comprises a dominant azimuthal flow, driven by the rotation of the shaft, with a weaker secondary flow comprising a single recirculation zone. The recirculation is in the anti-clockwise direction as a result of the chamber asymmetry, driven by the sealing air. The axial and radial components of the air velocity are typically an order of magnitude smaller than the azimuthal component. The computational results of the airflow show good qualitative agreement with the experimental results of Gorse et al [19] as shown by the vector plots of the secondary airflow given in Fig. 3.

The predicted trajectories are shown in Fig. 4 for oil droplets having diameters larger than 25μm. It is observed that there is no appreciable difference in the oil droplet motion with initial release location around the bearing cage. The large initial azimuthal component of the velocity means that the oil droplets travel in a predominantly straight line until they impact with the wall film on the chamber housing, where the majority have sufficient energy to promote splashing. This results in several smaller droplets being ejected back into the core flow, a significant proportion of which have diameters less than 25μm. These droplets are strongly affected by the core airflow and travel several circuits of the chamber before again impinging on the wall, or exiting the chamber through the vent pipe with the air. For engine design this is undesirable as it results in greater opportunity for heat exchange with the hot sealing air and increased residence time.

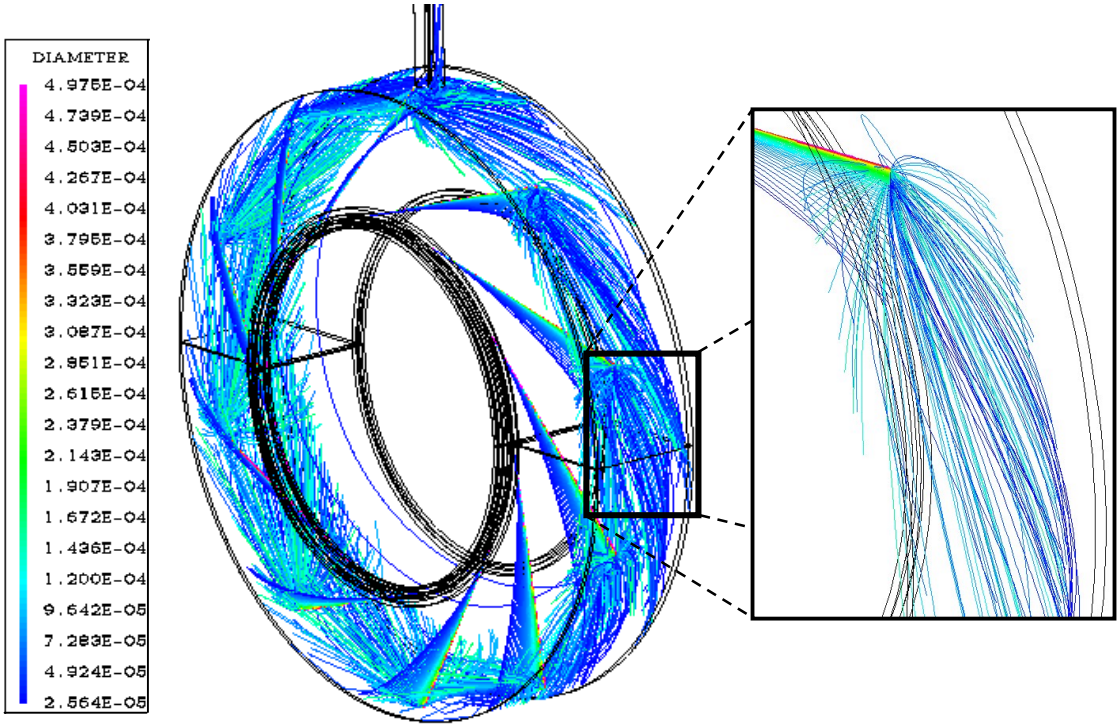

Figure 4. Predicted oil droplet trajectories in the chamber corresponding to droplets having diameters larger than 25μm.

A contour plot of the calculated distribution of the oil film thickness with circumferential and axial position is given in Fig. 5. A number of physical features are identifiable: Firstly, the oil film thickness profile in the azimuthal direction has two maxima, corresponding to angular locations of $\theta = 0$ and $\theta = \pi$, and two minima, corresponding to the angular locations of the vent and scavenge pipes. This agrees qualitatively with experimental measurements obtained in a former European project, exhibiting the same trend in the azimuthal profile. An axial variation in the film thickness is also observed, resulting from the combined effect of the secondary surface shear on the film and the additional axial momentum supplied to the film by the impinging droplets. These droplets also provide a source of mass to the wall film, the effect of which is observed in the region of the primary impact, z = 0.02 m, by the local increase in predicted film thickness.

5. Conclusions

A composite numerical model combining a commercial CFD code with sub-models for oil droplet/film interaction and the motion of the oil film has been presented. Preliminary results show that oil droplets shed from the bearing cage have sufficient energy on impact with the chamber housing and any associated wall film to promote splashing. As a result, droplets having smaller diameters (more likely to be affected by the rotating airflow) are ejected back into the core flow. This increases both the residence time of the oil in the chamber and the proportion of the oil carried by the sealing airflow through the vent pipe. The model provides valuable information regarding the film thickness distribution around the chamber housing along with the effect of geometric features such as vent and scavenge pipes that can be used for future heat transfer studies.

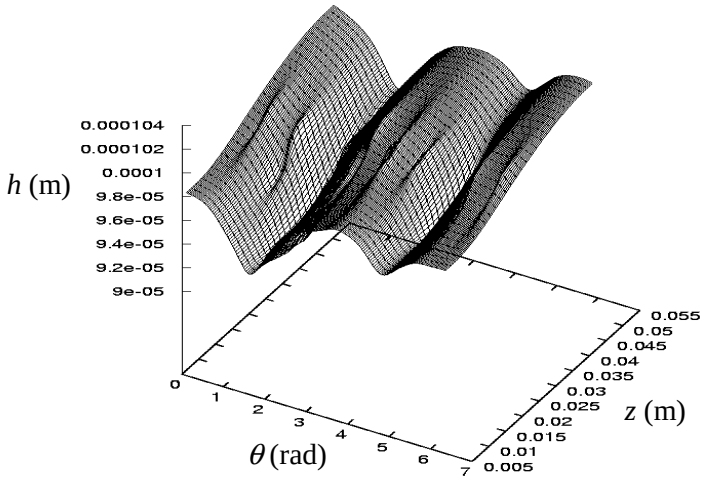

Figure 5. Oil film thickness distribution on the chamber housing.

6. Acknowledgements

The work has been supported by the European commission within the research project ATOS (Advanced Transmission and Oil System concepts), contract G4RD-CT-2000-00391. This financial support is gratefully acknowledged.

7. References

[1] Wittig S Glahn A Himmelsbach J 1993 ASME paper 93-GT-209
[2] Glahn A Wittig S 1999 Int. J. Rotating Machinery **5**(3): 155-165
[3] Glahn A Wittig S 1996 ASME Journal of Engineering for Gas Turbines and Power **118**(3): 578-583
[4] Chew JW 1996 ASME 96-GT-300
[5] Farrall M Hibberd S Simmons K 2000 Proceedings of the ASME FEDSM 2000 June 11-15 Boston Massachusetts USA
[6] Glahn A Busam S Wittig S 1997 ASME 97-GT-261
[7] Busam S Glahn A Wittig S 2000 ASME Journal of Engineering for Gas Turbines and Power **122**: 314-320
[8] Farrall M 2000 PhD Thesis University of Nottingham UK
[9] Naber JD Reitz RD 1988 SAE paper 880107
[10] Wang DM Watkins AP 1993 *Int. J. Heat and Mass Transfer* **14**(3): 301-312
[11] Senda J Kobayashi M Fukimoto H 1994 *SAE paper 941894*
[12] Bai C Gosman AD 1995 *SAE paper 950283*
[13] Stanton DW Rutland RJ 1996 *SAE paper 960628*
[14] Samenfink W Hallmann M Elsäßer A Wittig S 1994 ICLASS-94 Rouen France July
[15] Samenfink W Elsäßer A Dullenkopf K Wittig S 1999 Int. J. Heat and Fluid Flow **20**: 462-469
[16] Schmehl R Rosskamp H Willmann M Wittig S 1999 Int. J. Heat and Fluid Flow **20**: 520-529
[17] Liska R Wendroff B 1999 Int. J. Numer. Meth. Fluids **30**: 461-479
[18] Glahn A Kurreck M Willmann M Wittig S 1995 ASME paper 95-GT-100
[19] Gorse P Willenborg K Busam S Ebner J Dullenkopf K Wittig S 2003 Proceedings of the ASME Turbo Expo 2003 June 16-19 Atlanta Georgia USA